Inverse Radon Transform Based Micro-Doppler Analysis from a Reduced Set of Observations

Ljubiša Stanković[1], *Fellow IEEE,* Miloš Daković[1], *Member IEEE,* Thayananthan Thayaparan[2], *Senior Member IEEE,* Vesna Popović-Bugarin[1], *Member IEEE*

***Abstract*—A method for accurate and efficient parameter estimation and decomposition of sinusoidally frequency modulated signals is presented. These kinds of signals are of special interest in radars and communications. The proposed method is based on the inverse Radon transform property to transform a two-dimensional sinusoidal pattern into a single point in a two-dimensional plane. Since the signal is well concentrated (sparse) in the inverse Radon transform domain its reconstruction can be performed from a reduced set of observations (back-projections). Theory is illustrated on signals with one and more components, including noise and disturbances, as well as time-frequency patterns that deviate from sinusoidal form.**

***Keywords*— Frequency modulation, Parameter estimation, Radon transform, Time-frequency signal analysis**

I. Introduction

Sinusoidally frequency modulated (FM) signals appear in many applications, such as radars and communications. In radar signal processing, fast rotating, vibrating or oscillating parts reflect a signal causing micro-Doppler (m-D) effect in a form of sinusoidally FM signal [1]-[8]. In practice, it is very important to extract, decompose, and estimate parameters of these kinds of signals, since they are related to the physical dimensions and other properties of the moving objects [9]-[26]. Most of the techniques used for the detection, extraction and parameter estimation of these signals are based on two approaches. One is the parametric approach when the form of a signal, we are looking for, is assumed and we try to extract a desired component by matching its parameters [27], [28]. The other approach is based on the L-statistics and time-frequency (TF) analysis to extract non-stationary features from the TF representation of a composite signal. This method just separates stationary and non-stationary parts, but it does not separate non-stationary components within the signal [29], [30].

In this paper, we will present a method for analysis of sinusoidally FM components based on the inverse Radon transform (IRT) of signal's TF representation. The Radon transform, widely used in computer imaging applications (computed tomography), is also used in TF for projecting Wigner distribution in order to detect linear FM signals [31]-[34]. The Radon transform of a two-dimensional (2D) function, for a given angle, is defined by a projection (line integrals) onto the line with the same angle. The maximal value of the projections in the Radon transform is obtained for an angle when the integration line coincides with a signal component direction. In this case a line structure in the TF plane is projected into a point in the Radon transform. Thus, the direction of the linear FM signal can easily be estimated by varying the projection angle and calculating the Radon transform of the Wigner distribution. By detecting the Radon transform with the highest concentration (its maximum) the chirp rate value of a linear FM signal can be estimated. The fractional Fourier transform (FrFT) and the local polynomial Fourier transform (LPFT) are also used for the parameter estimation of the linear FM signals [38], [39]. They could be applied in similar scenarios as the Radon transform of the TF. Moreover, these methods are equivalent to each other, as it will be explained in Section III, [40], [41], [42]. The FrFT and LPFT are used for estimation of a vibration signature (TF signature of a sinusoidal FM signal) as well. To this aim, a nonstationary signal, corresponding to a vibrating object, is analysed within short time intervals so that in each analysed interval (subaperture) it can be approximated as a linear FM signal [38], [39]. The FrFT is then applied to estimate the local chirp rate in subapertures, with appropriate shifts along time. In the method proposed in [38], the duration of subapertures should be much smaller than the duration of the analysed vibration so that the linear FM approximation of the analysed signal part holds in the subaperture.

Here, we will use the IRT rather than the Radon transform of TF representation. The Radon transform of a 2D function containing a 2D delta function is a sinusoidal pattern with an amplitude corresponding to the distance of the point from the origin and the initial phase corresponding to the angle of the point position. It is obvious that a sinusoidal pattern in the TF plane (TF representation of sinusoidally FM signal) will project to a 2D delta pulse in the IRT. In the IRT, the sinusoidal TF forms of any duration will transform to a point, without the assumption about linearity in the considered interval. Thus, the entire signal's energy from the TF domain is projected into a single point in the IRT domain. Behavior of the Radon transform and the inverse Radon transform is completely different, in contrast, for example, to the Fourier transform [44]. Unlike in the Radon transform of TF representation (or the FrFT or LPFT) where a sinusoidally FM signal must be analysed within short intervals so that linear FM law can be assumed, in the algorithm proposed here, the IRT is applied on this kind of signals without linearity assumption.

The initial idea for using the IRT was presented in [30],

[1] University of Montenegro, Podgorica, Montenegro, email: {ljubisa, milos, pvesna}@ac.me, +38267234430,

[2] Research and Development Department, Ministry of Defence, Ottawa, Canada, email: Thayananthan.Thayaparan@drdc-rddc.gc.ca

This research is supported by the project "New ICT Compressive Sensing Based Trends Applied to: Multimedia, Biomedicine and Communications (CS-ICT)" (Montenegro Ministry of Science, Grant No. 01-1002).

with more details in [45]. In [30], the IRT is used for the m-D separation from a rigid body. In the case of multiple rotating reflectors, multiple peaks will be detected in the IRT, therefore, by filtering the region around each peak and calculating RT of the filtered IRT, TF representation of the signal resulting from the rotating parts is obtained [45]. The basic idea from these two papers is further developed and presented here. In this paper, a property that the IRT of a TF representation of a sinusoidally FM signal is well concentrated (sparse) is used to perform analysis and reconstruction from a few back-projections (observations). It is shown that in an ideal case just three observations in the IRT would be sufficient to reconstruct more than one sinusoidal pattern in image. The robustness of the proposed technique is tested through examples with noisy signals with a various number of observations. Disturbances in a form of flashes, rigid body reflection and noise, are considered in this paper as well. The method is applied on the benchmark data set of Iroquois helicopter simulations.

The paper is organized as follows. The signal model of the m-D effect is introduced in Section II. The IRT is reviewed in Section III. A method for estimation of the sinusoidally FM signal's parameters is the topic of Section IV. The examples that illustrate the efficiency of the presented method are given in Section V. The conclusion is given in Section VI.

II. Signal Model

In the ISAR (Inverse Synthetic Aperture Radar) case, the aim is to obtain a high-resolution image of a target based on the change in viewing angle of the target with respect to the fixed radar. The received signal usually contains a rigid body part and an m-D part. Here we will ignore the rigid body part in the analysis, and consider only the m-D components.

In the case of K fast rotating m-D points, the received signal can be written as [29]

$$s(t) = \sum_{k=1}^{K} \sigma_{Rk} e^{j2[y_{R0k}\omega_B t + A_{Rk}\sin(\omega_{Rk}t)]\omega_0/c}, \qquad (1)$$

where ω_{Rk} is the angular frequency of the k-th m-D point, A_{Rk} is the rotation amplitude, y_{R0k} is the center of rotation, ω_B is the angular velocity of the rigid body with respect to radar, σ_{Rk} is the reflection coefficient, ω_0 is the radar operating frequency and c is the propagation speed (speed of the light).

If a reflecting point vibrates, around a central point (x_{R0k}, y_{R0k}), along a line parallel to the line-of-sight, with the frequency ω_{Vk}, reaching the maximum amplitude A_{R_k} from the central point, then we get the form as (1), with the last phase term $A_{Rk}\sin(\omega_{Rk}t)$ being replaced by $A_{Rk}\sin(\omega_{Vk}t)$. Thus, the vibrations can be analysed in the same way as the rotations.

In the case of many rotating/vibrating reflectors, the resulting signal is a sum of sinusoidally FM components. The instantaneous frequency of each component is equal to the phase derivative

$$\Omega_k(t) = 2[y_{R0k}\omega_B + \omega_{Rk}A_{Ri}\cos(\omega_{Rk}t)]\omega_0/c.$$

In the Fourier domain, the components are approximately located within the frequency range from $2[y_{R0k}\omega_B - \omega_{Rk}A_{Rk}]\omega_0/c$ to $2[y_{R0k}\omega_B + \omega_{Rk}A_{Rk}]\omega_0/c$. An ideal TF representation should concentrate the signal energy along the instantaneous frequency. It should be of the form

$$ITF_k(t,\Omega) \sim 2\pi\sigma_{Rk}^2\delta(\Omega - \Omega_k(t)). \qquad (2)$$

In the next section it will be shown that this representation is transformed into a single nonzero point by using the IRT. The IRT of TF representation of these kinds of signals is the domain where it is sparse. The sparsity of the IRT presentation means here that the number of sinusoidal components is much fewer than the total number of points in the radar image and the corresponding IRT of this image.

Any TF representation concentrating the signal energy along the instantaneous frequency in the TF plane can be used as an approximation of (2), [42]. The spectrogram, as the simplest TF representation, is defined as a squared modulus of the short-time Fourier transform (STFT). In the discrete domain it reads

$$SPEC(n,l) = |STFT(n,l)|^2$$
$$STFT(n,l) = \sum_{m=0}^{N_w-1} w(m)x(n+m)e^{-j\frac{2\pi}{N_w}ml},$$

where $w(n)$ is the analysis window of the length N_w.

The S-method is used to improve the concentration of the spectrogram along the instantaneous frequency in the TF plane. It is defined as [42], [43]

$$SM(n,l) = |STFT(n,l)|^2$$
$$+2\,\mathrm{Re}\left\{\sum_{i=1}^{L} STFT(n,l+i)STFT^*(n,l-i)\right\}, \qquad (3)$$

where L is the number of correcting terms with respect to the spectrogram $|STFT(n,l)|^2$. It can significantly improve the TF representation concentration toward the ideal one with just a few of correcting terms. Further concentration improvement can be achieved by using higher-order TF representations.

III. Radon and Inverse Radon Transform Review

A review of the IRT is presented next, in order to show that a TF representation of a sinusoidally modulated signal will be transformed into a point and to relate the position of this point to the signal parameters.

A projection of a 2D function $f(x,y)$ onto the x-axis is

$$R_f(x) = \int_{-\infty}^{\infty} f(x,y)dy. \qquad (4)$$

A rotated version of a 2D function may be described in a rotated coordinate system using the coordinate transform. For a rotation angle β, it reads

$$\begin{bmatrix} \xi \\ \zeta \end{bmatrix} = \begin{bmatrix} \cos(\beta) & \sin(\beta) \\ -\sin(\beta) & \cos(\beta) \end{bmatrix} \begin{bmatrix} x \\ y \end{bmatrix}.$$

The projection of a function $f(x,y)$ onto ξ, with a varying rotation angle β, is the Radon transform of $f(x,y)$

$$R_f(\xi,\beta) = \int_{-\infty}^{\infty} f(\xi,\zeta)d\zeta, \qquad (5)$$

where $f(\xi,\zeta)$ is the 2D function $f(x,y)$ in the rotated system,

$$f(\xi,\zeta)=f(x\cos\beta+y\sin\beta,-x\sin\beta+y\cos\beta).$$

The Radon transform is periodic in β with 2π. Projections for $0\leq\beta<\pi$ are sufficient to calculate all transform values. By knowing all projections, for $0\leq\beta<\pi$, we can reconstruct a 2D function $f(x,y)$ from its projections (basic theorem for computed tomography) [44].

Let us consider a simple setup where the analysed image is a 2D delta function located at the point $f(x,y)=\delta(x-x_0)\delta(y-y_0)$ in the x,y domain. For an arbitrary direction a projection of the function $f(\xi,\zeta)=\delta(\xi-\xi_0)\delta(\zeta-\zeta_0)$ onto ξ, with $\xi_0=x_0\cos(\beta)+y_0\sin(\beta)$, $\zeta_0=-x_0\sin(\beta)+y_0\cos(\beta)$, results in the Radon transform

$$R_f(\xi,\beta)=\int_{-\infty}^{\infty}f(\xi,\zeta)d\zeta=\delta(\xi-\xi_0) \tag{6}$$
$$=\delta(\xi-(x_0\cos(\beta)+y_0\sin(\beta)))=\delta(\xi-A\cos(\beta+\psi)).$$

Note that this is a sinusoidal pattern in a 2D (ξ,β) domain, with the amplitude $A=\sqrt{x_0^2+y_0^2}$ and the phase $\psi=\arctan(y_0/x_0)$. Thus, a point in the (x,y) domain transforms to a sinusoidal pattern in the Radon transform domain. It means that a sinusoidal pattern will be transformed into a point by using the IRT

$$\delta(\xi-A\cos(\beta+\psi))\underset{RT}{\overset{IRT}{\rightleftarrows}}\delta(x-x_0)\delta(y-y_0).$$

When all signal energy is concentrated into a point, then its parameter estimation is very robust and reliable. Moreover, just three parameters are to be estimated meaning that three independent observations will be sufficient. In addition, if we will be able to associate parameters from one back-projection to different sinusoidal patterns, then three observations will be sufficient for more than one sinusoidal pattern analysis.

Since the Radon transform has already been used in the TF analysis, including the analysis of radar signals, here we will explain the crucial difference between the Radon transform behavior and the IRT used in this paper. The Radon transform projects a 2D signal. A projection is calculated as an integral (5) along the straight lines, whose direction is defined by the projection angle β. As such, it can be used (and it has been used) for the detection of straight line structures in the 2D image. In the TF analysis, straight line structures correspond to the linear FM signals. When the projection line coincides with a TF structure of a liner FM signal (linear structure), then the projection (line integral) value is large. For any other direction of the integration, not corresponding to the TF structure of a linear FM signal, the projection (line integral) assumes much smaller values. This was the basis for the Radon transform application in the detection of the linear FM signals in a TF representation [31]-[34].

This property of the Radon transform is directly related to the FrFT, defined by

$$X_\beta(t)=\sqrt{\tfrac{1-j\cot\beta}{2\pi}}e^{j\frac{\cot(\beta)}{2}t^2}\int_{-\infty}^{\infty}x(\tau)e^{j\frac{\cot(\beta)}{2}\tau^2}e^{-jt\tau\csc\beta}d\tau. \tag{7}$$

It is well known that the fractional Fourier transform rotates the TF plane [40], [41]. If a fractional Fourier transform is calculated with a parameter β and then the 2D TF representation is calculated using the FrFT of the signal, it is the same as if the 2D TF representation is calculated based on the signal and the TF representation is rotated by the angle β. In symbolic notation:

if $f(t,\Omega)=\mathrm{TF}\{x(t)\}$
then $\mathrm{TF}\{X_\beta(t)\}=f(t\cos\beta-\Omega\sin\beta,t\sin\beta+\Omega\cos\beta)$

Having in mind that the projections of the TF representations are equal to their marginal properties, then instead of calculating the TF representation and then its Radon transform, the same result will be obtained by calculating the FrFT and taking its squared moduli

$$R_f(\xi,\beta)=\left|X_\beta(\xi)\right|^2.$$

The squared moduli of the FrFT are the projections (marginal properties) of the rotated TF representations (their Radon transforms). This procedure can be further simplified by using the fact that the FrFT defined by (7) is just a scaled Fourier transform of the signal multiplied by a linear FM signal, $\mathrm{FT}\{x(\tau)e^{j\frac{\cot(\beta)}{2}\tau^2}\}$. The FrFT can directly be related to the first-order polynomial Fourier transform (PFT) as

$$X_\beta(t)=\sqrt{\tfrac{1-j\cot\beta}{2\pi}}e^{j(t^2/2)\cot\beta}PFT_{-\cot(\beta)/2}(t\csc(\beta))$$
$$PFT_{\Omega_1}(\Omega)=\int_{-\infty}^{\infty}x(\tau)e^{-j(\Omega\tau+\Omega_1\tau^2)}d\tau.$$

Thus, we may say that the calculation of the Radon transform of a TF representation or the fractional Fourier transform or the first-order polynomial Fourier transform of a signal reduces to:

1. Multiplication of a signal $x(t)$ by $e^{-j\Omega_1\tau^2}$ (de-chirping)
2. Fourier transform calculation of the de-chirped signal.

Based on this, we come again to the same conclusion as the one drawn from the geometry of the Radon transform. These techniques are optimal for the linear FM signals. They are used for analysis of these signals in [31]-[34], including the signals that can be approximated by linear FM signals within the considered time interval. These methods are not appropriate for nonlinear structures, like for example, sinusoidal structures in the TF representation, corresponding to the m-D effect.

In contrast to the Fourier transform, when the properties of the direct and inverse transform are similar, the inverse Radon transform is a completely different from the direct Radon transform. Its calculation is based on back-projecting of one dimensional forms to two dimensions of the original signal. An elementary 2D delta-pulse like structure (the sparsiest possible form of a function) will back-project into a sinusoidal form in the original domain. It is important to note that this kind of TF representations (2D delta-pulse like TF representation) is not considered in the literature due to a simple reason that it does not exist (uncertainty principle would be violated). However, a sinusoidal pattern in the IRT domain exists as a TF representation. It is then back-projected to a 2D delta-pulse like form, which is not a TF representation. Therefore the uncertainty principle is not violated in this case. This is

the reason why the traditional research related to the direct Radon transform cannot be related to the theory presented in this paper and the reason why the IRT is proposed as the main tool for the m-D structure analysis.

IV. Parameter Estimation using the Inverse Radon Transform

Consider a multicomponent signal

$$x(t)=\sum_{k=1}^{K}A_x^{(k)}\exp\left(j\frac{A_m^{(k)}}{f_m^{(k)}}\sin(2\pi f_m^{(k)}t+\theta_m^{(k)})\right)+\varepsilon(t), \tag{8}$$

with K sinusoidally FM components. Disturbing components and noise are denoted by $\varepsilon(t)$. A TF representation $T(t,\Omega)$ of a given signal concentrates its energy along the components' instantaneous frequencies

$$\Omega_k(t)=2\pi A_m^{(k)}\cos(2\pi f_m^{(k)}t+\theta_m^{(k)}).$$

Therefore, this signal is presented in (t,Ω) plane by K sinusoidal patterns.

If we change the time coordinate with $\varphi=2\pi f_m^{(k)}t$, then, based on the analysis in the previous section, we can conclude that in the IRT of the obtained TF representation-based image $T(\varphi/(2\pi f_m^{(k)}),\Omega)$ we will have at least one highly concentrated peak (point) that corresponds to the k-th sinusoidal pattern. Its distance from the origin corresponds to the modulation parameter $A_m^{(k)}$ and the angle of the point is equal to $\theta_m^{(k)}$. In this way, we can accurately estimate the modulation parameters $A_m^{(k)}$ and $\theta_m^{(k)}$.

The modulation parameter $f_m^{(k)}$ can be estimated by introducing a change of coordinate from t to φ, as $\varphi=\alpha t$ where α is a parameter. Now we can vary the parameter α within a range of possible values and search for a value $\hat{\alpha}^{(k)}$ that produces an IRT with a highly concentrated peak. In that case, we know that $\hat{\alpha}^{(k)}=2\pi f_m^{(k)}$ and we can estimate the modulation parameter $f_m^{(k)}$. The range of α should be wide enough to include $2\pi f_m^{(k)}$. Its limits could be determined as the minimal and the maximal expected $2\pi f_m^{(k)}$ in the considered case.

Since the IRT in the case of $\hat{\alpha}^{(k)}=2\pi f_m^{(k)}$ is highly concentrated for k-th component, the concentration measures [35] can be used to detect the event when $\hat{\alpha}^{(k)}$ is found.

In the considered multicomponent case, the concentration measure of the obtained IRT can produce several or all K values of α with visible and distinguishable concentration measure peaks. Then, these values are associated to the corresponding signal parameter $f_m^{(k)}$, while $A_m^{(k)}$ and $\theta_m^{(k)}$ are calculated from the position of maximum in the IRT calculated for $\hat{\alpha}^{(k)}$, i.e. IRT of $T(\varphi/\hat{\alpha}^{(k)},\Omega)$. However, due to different amplitudes and different number of periods in the TF plane, usually only the strongest component is visible in the concentration measure.

In general, two approaches are used to measure the concentration of a signal transform. One is based on the measuring transformation spread. The basic idea for this measures comes from counting nonzero values using the L_0-norm of the transformation. However, this kind of norm is difficult for optimization and sensitive to any disturbance. That is why measures of the form [35]

$$\mathcal{M}_p^p=\left(\sum_n\sum_k|IRT(n,k)|^{1/p}\right)^p$$

are used with $1\leq p<\infty$. The most widely used norm, within this approach, is obtained with $p=1$. This kind of norm dominates the optimization problems in compressive sensing [36], [37].

The other approach to measure the transformation concentration is based on measuring its peakedness, with a normalized transformation energy. Then, higher order powers of the transformation are used. This kind of concentration measures are used in the TF adaptive kernel design. This approach is especially interesting if we look for a very peaked form of the transformation, like in the IRT case. A limit case of this approach is the concentration measure obtained for $p\to 0$, i.e. $1/p\to\infty$. The concentration measure, in this limit case, equals to

$$\mathcal{M}=\lim_{p\to 0}\left(\sum_n\sum_k|IRT(n,k)|^{1/p}\right)^p=\max\left\{|IRT(n,k)|\right\}.$$

In our previous work [45], the normalized measure $\mu=\mathcal{M}_1^1/\mathcal{M}_{1/2}^{1/2}$ was used. It was based on the first approach and was more sensitive to the disturbances presence. In our research afterwords, we have found the measure based on maxima (corresponding to L_∞-norm) is more robust and the best suited for a single maximum detection in the IRT function.

A. Algorithm

The estimation algorithm is summarized as:

Step 1. Start from the signal $x(n)$ with unknown modulation parameters and unknown number of components. Assume that the modulation frequency satisfies $f_{\min}\leq f_m\leq f_{\max}$, where $f_{\min}$ and $f_{\max}$ are constants. Set the number of estimated components to $k=0$.

Step 2. Set $k=k+1$ and repeat the following steps if the energy of the signal $x(t)$ is not negligible or if it is higher than the expected noise energy.

Step 3. Calculate the TF representation $T(t,\Omega)$ of $x(n)$. Here we can use any TF representation concentrating the signal energy along the instantaneous frequency in the TF plane [42]. The result of this step is a 2D TF image of the considered signal.

Step 4. Consider a set of possible α as M equally spaced values between $2\pi f_{\min}$ and $2\pi f_{\max}$. For each α within the considered set, introduce coordinate change $\varphi=\alpha t$ and calculate the IRT of the image $T(\varphi/\alpha,\Omega)$.

Step 5. Calculate the concentration measure $\mathcal{M}$ of the obtained IRTs for each α and find $\hat{\alpha}^{(k)}$ that produces the highest concentration.

Step 6. Estimate the modulation frequency of the k-th component as $\hat{f}_m^{(k)}=\hat{\alpha}^{(k)}/(2\pi)$.

Step 7. Find the position of the IRT maximum calculated with $\hat{\alpha}^{(k)}$, i.e. IRT of $T(\varphi/\hat{\alpha}^{(k)},\Omega)$. Denote the detected coordinates as $x_m^{(k)}$ and $y_m^{(k)}$.

Step 8. Estimate the modulation amplitude and phase of the k-th component as

$$\hat{A}_m^{(k)} = \sqrt{(x_m^{(k)})^2 + (y_m^{(k)})^2},$$
$$\hat{\theta}_m^{(k)} = \arctan(y_m^{(k)}/x_m^{(k)}).$$

Step 9. Filter out k-th component by demodulating current signal $x(n)$

$$x_d(n) = x(n) \exp\left(-j\frac{\hat{A}_m^{(k)}}{\hat{f}_m^{(k)}} \sin(2\pi \hat{f}_m^{(k)} n\Delta t + \hat{\theta}_m^{(k)})\right),$$

calculating the DFT of the demodulated signal $X_d(k) = \mathrm{DFT}[x_d(n)]$ and removing DC component by putting zero value to $X_d(0)$, and several neighboring points $X_d(1)$, $X_d(N)$, $X_d(2)$, $X_d(N-1)$ ... Calculate the filtered signal by the inverse DFT $x_f(n) = \mathrm{IDFT}[X_d(k)]$ and modulate it in order to cancel frequency shifts in the remaining components caused by the demodulation

$$x_m(n) = x_f(n) \exp\left(j\frac{\hat{A}_m^{(k)}}{\hat{f}_m^{(k)}} \sin(2\pi \hat{f}_m^{(k)} n\Delta t + \hat{\theta}_m^{(k)})\right).$$

Step 10. Set $x(n) = x_m(n)$ and go to **Step 2**.

The presented procedure can be used on periodic non-sinusoidally FM signals, producing non-sinusoidal patterns in the TF plane. The result will be the parameters of the closest sinusoidal pattern form, as it will be shown in the examples.

B. Analysis of the m-D from a Reduced Set of Observations

From the previous analysis, we can conclude that the m-D effect of rotating or vibrating parts is sparse in the IRT of its TF representation. Namely, in the IRT domain, with appropriate scaling parameter α, each m-D component is represented as a single nonzero value.

From the compressive sensing theory, we know that such signals can be analysed by using much smaller data sets i.e., we do not have to use the whole data set [36], [37]. In general, when we have data represented with N observations if there is a transformation domain where this data can be represented with K nonzero coefficients ($K \ll N$), then this data can be analysed by using only N_p observations $K < N_p < N$. For this kind of signal, we say that it is sparse in this transformation domain. Its processing is done within the framework of compressive sensing.

Consider the m-D effect caused by a single rotating/vibrating scatterer. Its ideal TF representation is sinusoidal pattern of the form

$$ITF(t,\Omega) \sim 2\pi\sigma_R^2 \delta(\Omega - (x_0\cos\beta + y_0\sin\beta)), \quad (9)$$

with $\beta = \alpha t$. The parameter α is used to transform the time axis from TF domain into angle in the Radon transform domain. This parameter is unknown and it equals to the angular frequency of the m-D component.

Let us consider just three TF observations of the m-D component at the instants t_1, t_2, and t_3

$$ITF(t_1,\Omega) \sim \delta(\Omega - \Omega_1)$$
$$ITF(t_2,\Omega) \sim \delta(\Omega - \Omega_2)$$
$$ITF(t_3,\Omega) \sim \delta(\Omega - \Omega_3).$$

These three observations correspond to three angles in the IRT

$$\beta_1 = \alpha t_1 \qquad \beta_2 = \alpha t_2 \qquad \beta_3 = \alpha t_3,$$

where parameter α is to be found.

In the IRT domain, we have system of three equations

$$x_0\cos\alpha t_1 + y_0\sin\alpha t_1 = \Omega_1$$
$$x_0\cos\alpha t_2 + y_0\sin\alpha t_2 = \Omega_2$$
$$x_0\cos\alpha t_3 + y_0\sin\alpha t_3 = \Omega_3.$$

Each equation presents a line in the IRT domain. Now we should find α when three lines intersect in a single point. By solving the system of two equations (first and second equation) for x_0 and y_0 we get

$$x_0 = \frac{\Omega_1\sin\alpha t_2 - \Omega_2\sin\alpha t_1}{\sin\alpha(t_2 - t_1)}$$
$$y_0 = \frac{\Omega_1\cos\alpha t_2 - \Omega_2\cos\alpha t_1}{\sin\alpha(t_1 - t_2)}. \quad (10)$$

Replacing these values into the third equation we get the solution

$$\Omega_1\sin\alpha(t_2 - t_3) - \Omega_2\sin\alpha(t_1 - t_3) = \Omega_3\sin\alpha(t_2 - t_1).$$

For the special case $t_2 = t$, $t_1 = t - \Delta_t$, and $t_3 = t + \Delta_t$ a simple solution for α follows

$$-\Omega_1\sin\alpha\Delta_t + \Omega_2\sin 2\alpha\Delta_t = \Omega_3\sin\alpha\Delta_t$$
$$\cos\alpha\Delta_t = (\Omega_1 + \Omega_3)/(2\Omega_2).$$

Here we should take care about $2p\pi$ ambiguity in solving for α, where p is an integer. After α is estimated, the m-D parameters are calculated as $A = \sqrt{x_0^2 + y_0^2}$ and $\theta = \arctan(y_0/x_0)$ with x_0 and y_0 obtained from (10).

In theory, with three close observations we can reconstruct one m-D component. For close observations there is no $2p\pi$ ambiguity in the solution of α [18]. In the case of K components, we will have ideal TF representation of the form

$$ITF(t,\Omega) \sim \sum_{k=1}^{K} 2\pi\sigma_{Rk}^2 \delta(\Omega - \Omega_k(t)). \quad (11)$$

If the observations are close enough and frequencies are sufficiently apart, we can easily distinguish sets $[\Omega_k(t_1), \Omega_k(t_2), \Omega_k(t_3)]$ for different k. Then the application of the presented one component case to a K component signal cases is straightforward. This approach can be extended to any three observations as far as we are able to correctly associate the frequencies $\Omega_k(t_1), \Omega_k(t_2), \Omega_k(t_3)$ to the corresponding m-D components (for example, by using component amplitudes).

Using more than three observations will improve possibility to resolve signal components. In the case of noisy data using more observations will also improve the reconstruction performance.

V. EXAMPLES

Example 1: Consider $N = 128$ samples of a multicomponent noisy signal consisted of $K = 3$ sinusoidally FM components of the form (8). The signal is sampled with $t = n\Delta t$, $\Delta t = 1/128$, $n = 0, 1, \ldots N-1$, while component parameters are:
$A_x^{(1)} = 1$, $f_m^{(1)} = 1.4$, $A_m^{(1)} = 50$, $\theta_m^{(1)} = 30^\circ$,
$A_x^{(2)} = 0.7$, $f_m^{(2)} = 0.8$, $A_m^{(2)} = 28.6$, $\theta_m^{(2)} = 180^\circ$,
$A_x^{(3)} = 0.7$, $f_m^{(3)} = 1$, $A_m^{(3)} = 35.7$ and $\theta_m^{(3)} = -60^\circ$.

The spectrogram and the S-method of the considered signal are presented in Figs. 1 (a) and (b). The spectrogram is calculated with a 17-point Hann window, while the S-method is calculated with a 55-point Hann window and $L = 8$. In both cases, the TF representation is calculated at each available time instant. The Radon transforms of the spectrogram and the SM, calculated for β from 0 to 180 degrees with one degree step, are presented in Figs. 1 (c) and (d) respectively. The Radon transform of TF representation (at an angle β) is a projection onto the line with an angle β. Since the considered TF representation is consisted of sinusoidal patterns, there are no sharp peaks in the Radon transform. Slightly higher values in the Radon transform appear for angles β that coincide with the directions of the sinusoidal pattern that can be considered as locally linear. However, no conclusions about the sinusoidal pattern parameters can be made from Figs. 1 (c) and (d).

The Radon transform would project a linear pattern into a point. It could be used for the estimation of a linear FM direction, but not for the estimation of the sinusoidally FM patterns. For analysis of these signals we use the IRT. The parameter α is varied from 0.2 to 15 with step 0.2. For each α the IRT, along with the corresponding concentration measure, is calculated. The IRT of the spectrogram and the SM, calculated for $\alpha = 8.8$, producing maximum concentration measure $\mathcal{M}(\alpha)$, is presented in Figs. 1(e) and (f), respectively.

The presented algorithm estimates first the parameters of the strongest component, Figs. 1(g) and (h). The estimated parameters are

$$\hat{f}_m^{(1)} = 1.4, \quad \hat{A}_m^{(1)} = 48.50, \quad \hat{\theta}_m^{(1)} = 30.26^\circ.$$

The sinusoid that results from the estimated modulation parameters is depicted by dashed line over the spectrogram of the analysed signal in Fig. 1(g). The estimated modulation parameters correspond to the component instantaneous frequency. The concentration measure of the IRT, calculated for each value of α, is presented in Fig. 1(h). Its maximum is depicted by a circle. The first estimated component is filtered out and the next iteration of the presented algorithm is continued with $x(n) = x_m(n)$. The parameters of the second component are estimated next. Results are presented in Figs. 1 (i) and (j). The estimated modulation parameters are

$$\hat{f}_m^{(2)} = 0.80, \quad \hat{A}_m^{(2)} = 28.0, \quad \hat{\theta}_m^{(2)} = 180^\circ.$$

In the next step, the second estimated component is filtered out and the parameters estimation for the last component is done. The results are given in Figs. 1 (k) and (l). The estimated parameters are

$$\hat{f}_m^{(3)} = 0.99, \quad \hat{A}_m^{(3)} = 35.52, \quad \hat{\theta}_m^{(3)} = -58.4^\circ.$$

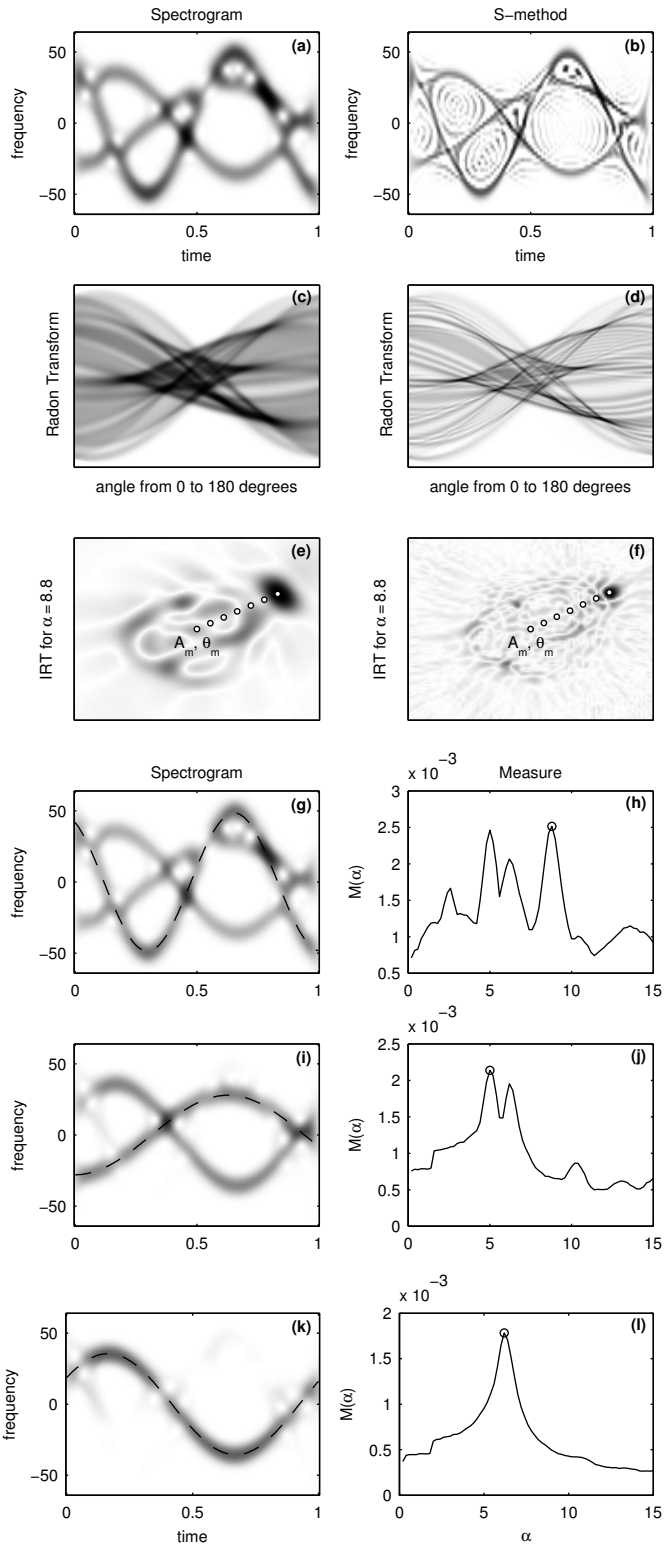

Fig. 1. Multicomponent signal example. Time-frequency representation: spectrogram (a), SM (b); Radon transform calculated for angles from 0 to 180 degrees, with one degree step (c), (d); inverse Radon transform with the highest concentration (e), (f). Estimation of the first component (g), (h); second component (i), (j); and third component (k) and (l). Each component is removed from the signal after estimation, according to the given algorithm, prior to next component estimation. Estimated modulation is plotted with dashed line over spectrogram image in (g), (i) and (k), while the maximum of the concentration measures given in (h), (j) and (l) is depicted by circle.

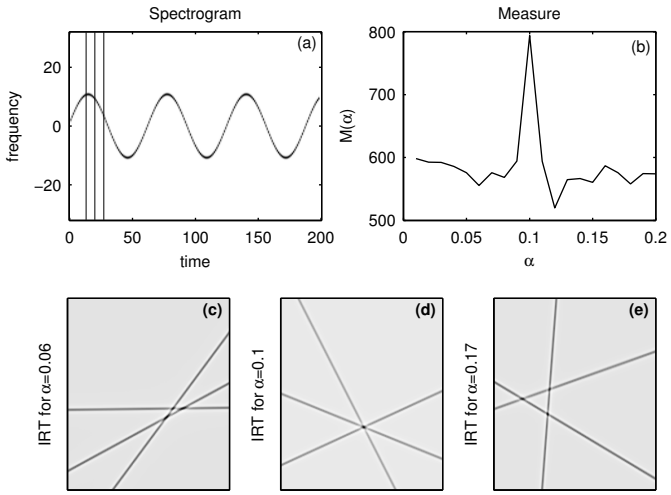

Fig. 2. Time-frequency representation of sinusoidal FM signal (a). Concentration measure of the inverse Radon transform calculated from three observations of the spectrogram (b). Inverse Radon transform calculated from three observations when parameter α is not optimally chosen (c), (e). Inverse Radon transform calculated from three observations with highest concentration (optimally chosen α) (d). Three vertical lines on the spectrogram in (a) represents positions (instants) of the three observations used in reconstruction.

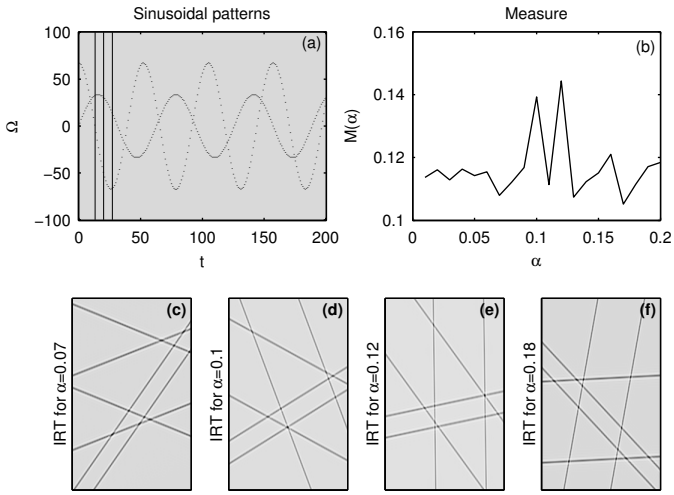

Fig. 3. Two sinusoidal patterns (a). Concentration measure for the inverse Radon transform calculated from three observations of sinusoidal pattern (b). Inverse Radon transform when parameter α is not optimally chosen (c), (f). Inverse Radon transform with optimally chosen α for the first sinusoidal pattern $\alpha = 0.1$ (d). Inverse Radon transform with optimally chosen α for the second sinusoidal pattern $\alpha = 0.12$ (e).

The agreement with the true parameters is high.

Example 2: The reconstruction procedure of one m-D component, based on three close observations of its TF representation, is illustrated in this example.

The analysed sinusoidal FM signal is of form (8) with $K = 1$, $\varepsilon(t) = 0$, $A_m = 10$, $f_m = 0.1/(2\pi)$, $\theta_m = 270°$, sampled with $\Delta t = 1/64$ and $64N$ samples in the total signal duration, with $N = 200$. The spectrogram is used as a TF representation. The STFT is calculated by using a Hann window with length $N_w = 129$, with the time step 64, so that we have N time instants in its spectrogram. This is presented in Fig. 2(a).

In the considered case, we can estimate all parameters of the analysed sinusoidal pattern (FM signal) by using only three observations of its TF representation. Green lines in Fig. 2(a) represent three values of β for which the observations of the considered TF representation are assumed to be available, i.e. $\beta_i = \alpha t_i$, $i = 1, 2, 3$. Then, the parameter α is varied from, for example, from 0.01 to 0.2 with a step of 0.01 and for each α the IRT and the corresponding concentration measure is calculated. The concentration measure $\mathcal{M}(\alpha)$, obtained by this procedure, is presented in Fig. 2(b) for the IRT calculated using only three observations of the spectrogram. Maximum at $\alpha = 0.1$ can easily be detected and the modulation parameters estimated from the IRT calculated by using this value of α, Fig. 2(d). In Figs. 2(c)-(e) the corresponding IRTs calculated for different values of α are presented. As it is expected from the previous theoretical analysis, in each IRT there are three lines, one line per available observation. All three lines intersect at a single point in the IRT for $\alpha = 0.1$ which is equal to the angular frequency of the analysed signal. The IRTs for values $\alpha \neq 0.1$ are depicted in Fig. 2(c), (e). In these cases there is no one-point intersection of all three lines as in Fig. 2(d).

Example 3: In this example, the sinusoidal patterns:

$$ITF(t, \Omega) = \sum_{k=1}^{K} \delta(\Omega - A_k \cos(\beta_k + \psi_k)) \qquad (12)$$

with $K = 2$, $N = 200$, $A_1 = N/6$, $A_2 = N/3$, $\beta_1 = 0.1t$, $\beta_2 = 0.12t$, $\psi_1 = 3\pi/2$, $\psi_2 = 0$ and $t = 0, 1, ..., N$ are considered and depicted in Fig. 3(a). The concentration measure of the IRT calculated by using three observations are presented in Fig. 3(b) for different values of α. Parameter α is varied from 0.01 to 0.2 with step 0.01. Two peaks at the positions, corresponding to the first and the second sinusoidal pattern, are clearly distinguishable. These values of α can be used for the IRT calculation and other modulation parameter estimation. Green lines in Fig. 3(a) represent time instants of the available observations of the considered sinusoidal pattern. For each observation, we have two non-zero values, one per sinusoidal pattern. From Figs. 3(c)-(f) we can see that in each IRT, calculated by using three observations, there are six lines (three per one sinusoidal pattern). Moreover, each set of these three lines which corresponds to one sinusoidal pattern has, for each value of α, a parallel counterpart that correspond to the other sinusoidal pattern. Consequently, they will never intersect each other. In addition, only for α that corresponds to the period of a sinusoidal pattern three lines that are related to that sinusoidal pattern intersect each other in a single point, Fig. 3(d) for $\alpha = 0.1$ and Fig. 3(e) for $\alpha = 0.12$. The modulation amplitude and phase of a component can be estimated from the position of the point where all three lines intersect.

In theory, three observations are sufficient to detect all m-D components. However, in practice, the sensitivity to any kind of noise or discretization error is high. By increasing the number of observations, the robustness of the proposed approach is improved.

Example 4: Consider a signal of form (8) composed of five sinusoidal FM components, with $K = 5$, $A_x^{(k)} = 1$ for each k, $A_m^{(k)} = 21$, for $k = 1, 4, 5$, $A_m^{(2)} = A_m^{(3)} = 42$, $f_m^{(1)} = 0.1/(2\pi)$, $f_m^{(2)} = 0.12/(2\pi)$, $f_m^{(3)} = 0.07/(2\pi)$, $f_m^{(4)} = 0.14/(2\pi)$, $f_m^{(5)} = 0.18/(2\pi)$, $\theta_m^{(k)} = 3\pi/2$, for $k = 1, 4, 5$, $\theta_m^{(2)} = \theta_m^{(3)} = 0$ sampled with $\Delta t = 1/128$, $N = 200$, and duration $128N$. Although, in theory, three observations are sufficient for detecting all the m-D components, in the case when there are several m-D components, a higher number of observations should be used. The results for the IRT calculated from twenty observations (back-projections) of spectrogram are presented in Fig. 4. The Hann window of the length $N_w = 513$ is used for the STFT calculation. The STFT is calculated with a time step of 128, so that we have N time instants in the corresponding spectrogram shown in Fig. 4(a). There are five clearly distinguishable peaks in the concentration measure, Fig. 4(b). Each of these peaks is at the value of α which corresponds to one of the five m-D components. Higher number of observations make easier to distinguish the concentration measure for α when all back-projections are crossing in one point. To that aim, the IRT calculated from twenty observations for α that corresponds to the second and the third m-D component are presented in Figs. 4(c), (e). One point, where all twenty observations of the m-D components with modulation parameter that correspond to $\alpha = 0.07$ and $\alpha = 0.1$, crossed each other, assumes significantly higher intensity than all others. When the value of α does not correspond to the modulation parameter of any analysed component, there are many points with similar intensity, Fig. 4(d).

Performance of the proposed technique in the case of noisy signal are tested for various numbers of available observations. They are presented in Fig. 4(f). For each signal-to-noise ratio (SNR) and for the numbers of observations $N_p = 10, 20, 50, 100,$ and $200,$ the percentage of properly detected components in 20 realizations is presented. From Fig. 4(f) we can conclude that the detection with a reduced number of observations is possible at high values of SNR. Increasing the number of available observations the detection percentage is improved at low SNRs.

Comparison of the L_1-norm based concentration measure used in [45] and the maximum (L_∞-norm) based measure is done for $N_p = 50$ observations. For low noise (high SNR) both of them behave in a similar way. However, the detection threshold is lower for the maximum (L_∞-norm) based measure for about 5 [dB], Fig. 4(g). Similar results would be obtained for other numbers of observations N_p.

Example 5: The robustness of the proposed technique to other common disturbances is tested in this example. A pattern of form (12) is used with $K = 9$, $A_k = N/3$, for $k = 1, 4, 5, 6, 9$, $A_2 = N/6$, $A_3 = 1.1N/3$, $A_7 = 0.9N/3$, $A_8 = 0.8N/3$, $N = 200$, $\beta_1 = 0.1t$, $\beta_2 = 0.12t$, $\beta_3 = 0.11t$, $\beta_4 = 0.07t$, $\beta_5 = 0.14t$, $\beta_6 = 0.16t$, $\beta_7 = 0.09t$, $\beta_8 = 0.15t$, $\beta_9 = 0.18t$, $\psi_1 = 3\pi/2$, and $\psi_k = 0$ for $k = 2, ..., 9$. Nine sinusoidal patterns are presented in Fig. 5(a). The concentration measure of the IRT calculated from 20 observations and for different values of α, where α is varied from 0.05 to 0.2 with step 0.001 is presented in Fig. 5(b). Nine clearly

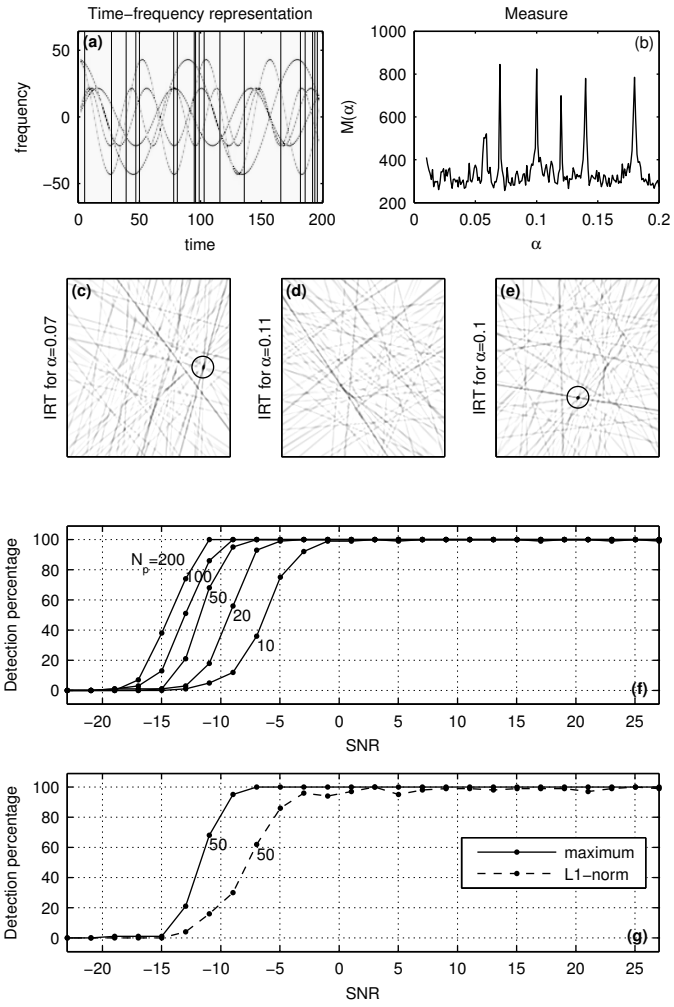

Fig. 4. Time-frequency representation of a signal composed of five sinusoidal FM components (a). Concentration measure for the inverse Radon transform calculated from $N_p = 20$ observations of the time-frequency representation at the positions indicated by vertical lines (b). Inverse Radon transform of 20 observations with optimally chosen α for the third sinusoidal pattern $\alpha = 0.07$ (c). Inverse Radon transform of 20 observations when parameter α is not optimally chosen (d). Inverse Radon transform of 20 observations with optimally chosen α for the second sinusoidal pattern $\alpha = 0.1$ (e). Percentage of detected components as a function of SNR for varying number of observations $N_p = 10$, 20, 50, 100, and 200 (f). Percentage of detected components as a function of SNR for $N_p = 50$ observations and two measures used for the detection: maximum (L_∞-norm) and L_1-norm (g). Statistical results are obtained by averaging over 20 realizations with random observation positions.

distinguishable peaks can be seen in this figure. Each peak is at a value of α that corresponds to the modulation parameter of a sinusoidal pattern. Nine sinusoidal patterns are analysed with 20 randomly selected observations to illustrate the proposed approach and its robustness to different kind of disturbances.

Common situation in the radar imaging is to have the m-D, rigid body reflectors and the flashes in the same image. In order to illustrate this scenario, the same nine component sinusoidal patterns are analysed in the presence of rigid body reflectors (horizontal lines) and flashes (vertical lines), Fig. 5(c). The concentration measure of the IRT of this kind of the signal, calculated for different values of α, is presented

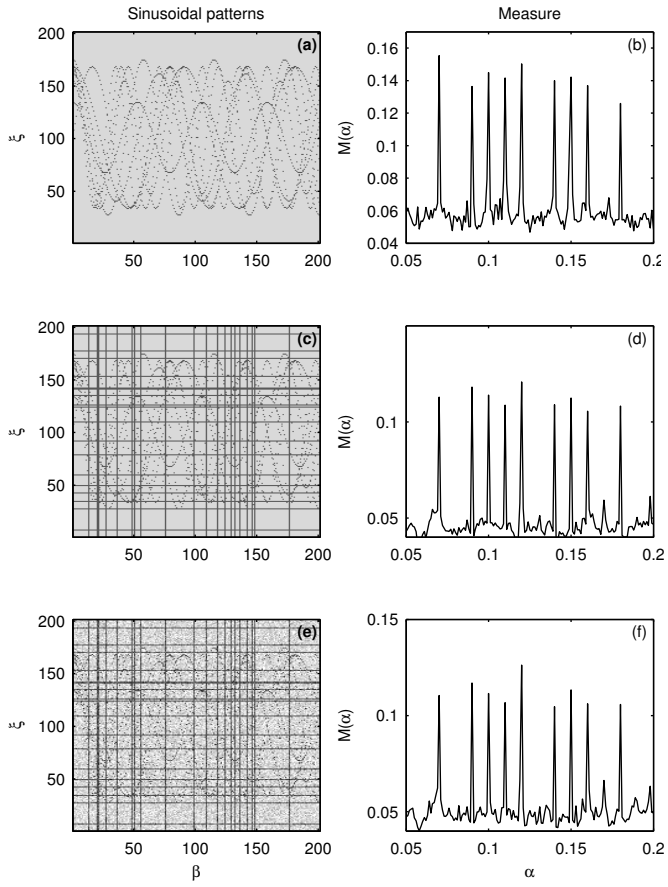

Fig. 5. Nine sinusoidal patterns (a). Concentration measure for the inverse Radon transform calculated by using 20 observations of the sinusoidal patterns (b). Nine sinusoidal patterns with rigid body reflectors and flashes (c). Concentration measure for the inverse Radon transform calculated by using 20 observations of the sinusoidal patterns with rigid body reflectors (d). Nine sinusoidal patterns with rigid body reflectors and flashes in the presence of Gaussian noise with $\sigma = 0.2$ (e). Concentration measure for the inverse Radon transform, calculated by using 20 observations of the sinusoidal patterns with rigid body reflectors and flashes in the presence of Gaussian noise with $\sigma = 0.2$ (f).

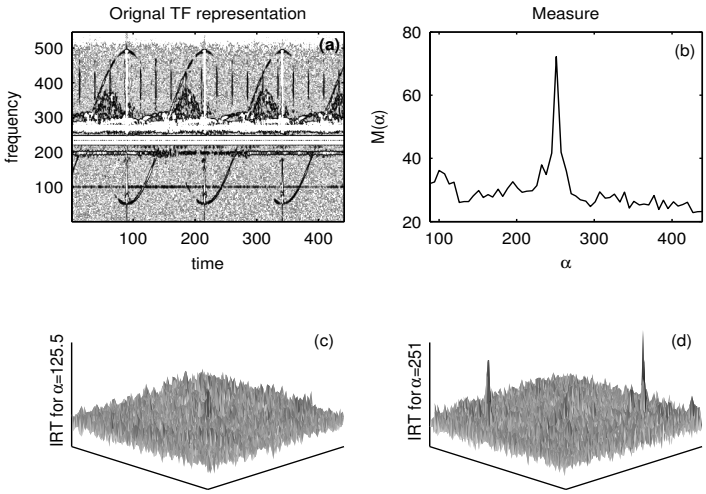

Fig. 6. German Air Force Bell UH-1D Helicopter. Image of the original TF representation, where the highest values are eliminated (a). Concentration measure for the inverse Radon transform calculated by using 300 observations (b). Concentration measure calculated for value of α which is not optimal (c). The IRT with optimally selected value of α (d) .

in Fig. 5(d). Despite the presence of significant disturbances caused by the rigid body reflectors and flashes, nine clearly distinguishable peaks, at the values of α which correspond to the nine sinusoidal patterns, are still visible. The IRT is calculated by using 20 observations, Fig. 5(c).

Now, the noise is added to this signal. In Fig. 5(e) the corresponding pattern obtained by adding a white Gaussian noise with $\sigma = 0.2$ is presented. The concentration measure of the IRT is presented in Fig. 5(f). Still we have nine distinguishable peaks, even with only 20 observations used for the IRT calculation.

Example 6: A benchmark data set for measuring the performance of this method that deals with the m-D is simulation of a German Air Force Bell UH-1D Helicopter known also as 'Iroquois', [29]. This is due to the fact that various effects are covered by this data set. In this example, we do not use the radar signal data, but rather the radar image from the literature, read as an image and loaded for the proposed method application as a matrix, Fig. 6(a). The stationary patterns along the time-axis correspond to the rigid body reflection. The motion of two main blades is manifested as two rotating reflectors, producing sinusoidal FM signals with a large magnitude in the frequency direction. The main rotor flashes are the signals producing lines that connect extreme points of the sinusoidal FM signal, along the time axis. The smaller pulses that can be seen on Fig. 6(a) correspond to the tail rotor flashes, [29].

We will show that even in this very complex case an analysis based on a reduced set of observations can be done. Here we will use 300 of available 441 observations for the IRT calculation. Concentration measure of the IRT calculated for $\alpha = 87.5$ to $\alpha = 439.25$ with a step of 6.2750 is depicted in Fig. 6(b). By comparing Fig. 6(a) and Fig. 6(b) it can be seen that the peak in the concentration measure of the IRT is obtained for $\alpha = 251$. It corresponds to the period of sinusoidal patterns in the TF representation used for the IRT calculation. We can see that two sinusoidal patterns are present in the TF representation (Fig. 6(a)), but only one peak appears in the measure of the IRT, Fig. 6(b). This is due to the fact that these sinusoidal patterns are with equal periods. However, in the IRT calculated for one $\alpha = 251$ two clear peaks appear, Fig. 6(d). The positions of these two peaks correspond to the amplitude and phase of the analysed sinusoidal patterns. For all other values of α, the measure does not detect a peak significantly higher than the other IRT values due to the fact that there are many different intersections of lines, but there is no intersection of 300 lines in single point, Fig. 6(c). Since a huge number of lines appears in the IRT calculated from 300 observations of this kind of signal, its 3D presentation is used here in order to increase the readability of the presentation.

Example 7: The presented estimation procedure could be used if the analysed signal is not sinusoidally modulated. We will illustrate this application through an example. Consider a

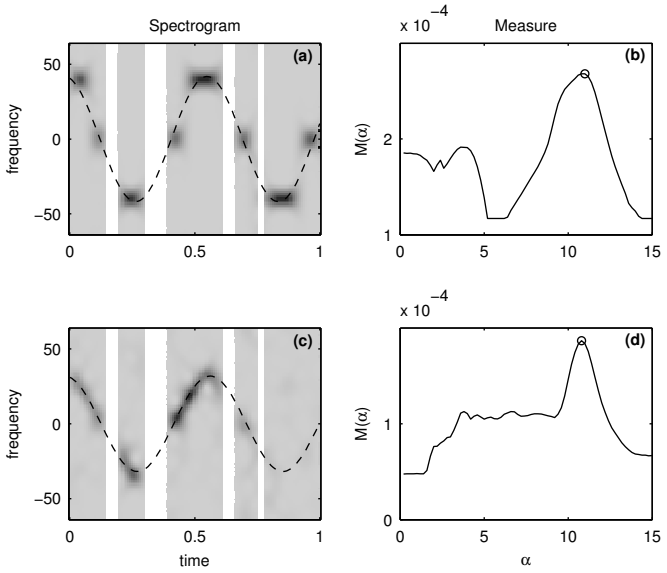

Fig. 7. Nonsinusoidal modulation: Frequency hopping signal (a), (b); Signal with triangular modulation and varying amplitude (c), (d).

frequency hopping signal

$$x_1(t) = \exp\left(j\int_0^t 250\,\mathrm{round}[\cos(3.6\pi u)]\,du\right),$$

where $\mathrm{round}[\cdot]$ operator rounds toward nearest integer, and a triangularly modulated signal $x_2(t)$ with a varying amplitude

$$x_2(t) = A(t)\exp\left(j\int_0^t 150\arcsin(\cos(3.6\pi u))\,du\right),$$
$$A(t) = \exp\left(-\left(\tfrac{t-0.35}{0.5}\right)^2\right).$$

We will also assume that some signal samples (about 20%) are unavailable. In this case, we can only calculate the spectrogram at the time instants/intervals when signal samples are available.

Although the proposed method is derived for sinusoidal modulations, the results presented in Fig. 7 clearly show that its applicability is not limited to the sinusoidal modulation patterns. Regions with unavailable samples are presented with white color in this figure. The estimated modulation parameters for the signal $x_1(t)$ are

$$\hat{f}_m = 1.75, \quad \hat{A}_m = 41.9, \quad \hat{\theta}_m = -14.0^\circ$$

and for the signal $x_2(t)$

$$\hat{f}_m = 1.72, \quad \hat{A}_m = 31.8, \quad \hat{\theta}_m = 12.6^\circ.$$

They agree with $f_m = 1.8$ in the considered signals. The closest estimated sinusoids are presented in Figs. 7 (a) and (c) as well.

Example 8: The spectrogram may not be a suitable tool for time-frequency analysis of the signal whose IF changes within the window are very fast. Then quadratic or other higher order time-frequency representations should be used. A very simple quadratic representation for improving the spectrogram based representation is the S-method, presented in Section II. In order to illustrate this situation consider a signal consisted of two sinusoidally FM components of the form (8), with a small noise $\varepsilon(t)$. The signal is sampled with $t = n\Delta t$, $\Delta t = 1/128$, $n = 0, 1, \ldots N-1$, where $N = 128$. The component parameters are:

$$A_x^{(1)} = 1, \quad f_m^{(1)} = 6, \quad A_m^{(1)} = 50, \quad \theta_m^{(1)} = 30^\circ,$$
$$A_x^{(2)} = 0.25, \quad f_m^{(2)} = 6.5, \quad A_m^{(2)} = 30, \quad \theta_m^{(2)} = 90^\circ.$$

The IF variations are fast in this case. The signal is analyzed using: the spectrogram with a narrow 21-point window, Fig. 8(a), and the S-method based improvement of the calculated spectrogram (with $L = 5$ terms, equation (3)), Fig. 8(b). Parameter α is varied from $1/15$ to 10 with step $1/15$. For each α, the IRT and its measure are calculated. The IRTs with the highest measures are presented in Figs. 8(c) and (d). Estimation of the first (stronger) component is presented in Fig. 8(e) and (f). After the parameter estimation, this component is removed from the analyzed signal and the parameters of the second component are estimated, Fig. 8(g) and (h). Since the IF variation are very fast the analysis based on the S-method is able to track these changes and to produce accurate results.

VI. Conclusion

A method for the parameter estimation of sinusoidally FM signals is introduced. The proposed method is based on the IRT and the concentration measures. It is shown that the proposed method provides promising estimation and decomposition results for monocomponent and multicomponent signals. In theory, since the TF representation of the m-D effect is sparse in the IRT domain, only three independent observations (back-projections) are sufficient to detect and reconstruct even more than one sinusoidally modulated pattern. In practice, a few observations are sufficient since the IRT domain is the domain of sparsity for these kinds of signals. The noise and the interferences influence to the estimation procedure is considered. It can be concluded that the proposed method is very robust to the noise and other interferences. We have also shown that the results obtained by the proposed method are meaningful even in cases when the analysed signal is periodic but not sinusoidally modulated. It can be used to estimate the parameters of periodic extension of a non-periodic TF patterns and partially available data as well.

References

[1] V. C. Chen, F. Li, S.-S. Ho, and H. Wechsler: "Analysis of micro-Doppler signatures," *IEE Proc. Radar, Sonar, Navig.*, vol. 150, no. 4, pp. 271-276, Aug. 2003.

[2] V. C. Chen: "Micro-Doppler effect in radar: Part I: Phenomenon, physics, mathematics, and simulation study," *IEEE Trans. on Aerosp. Electron. Syst*, vol. 42, no. 1 Jan 2006.

[3] X. Bai, F. Zhou, M. Xing and Z. Bao: "High resolution ISAR imaging of targets with rotating parts," *IEEE Trans. on Aerosp. Electron. Syst*, vol. 47, no. 4, pp. 2530 - 2543, Oct. 2011.

[4] F. Totir and E. Radoi: "Superresolution algorithms for spatial extended scattering centers," *Digital Signal Processing,* vol. 19, no. 5, pp.780-792, Sept. 2009.

[5] M. Martorella: "Novel approach for ISAR image cross-range scaling," *IEEE Trans. Aerosp. Electron. Syst.*, vol. 44, no. 1, pp. 281–294, 2008.

[6] M. Martorella and F. Berizzi: "Time windowing for highly focused ISAR image reconstruction," *IEEE Trans. Aerosp. Electron. Syst.*, vol. 41, no. 3, pp. 992–1007, 2005.

[7] Y. Wang and Y.-C. Jiang: "ISAR imaging of ship target with complex motion based on new approach of parameters estimation for polynomial phase signal," *EURASIP Journal on Advances in Signal Processing*, vol. 2011 (2011), Article ID 425203, 9 pages.

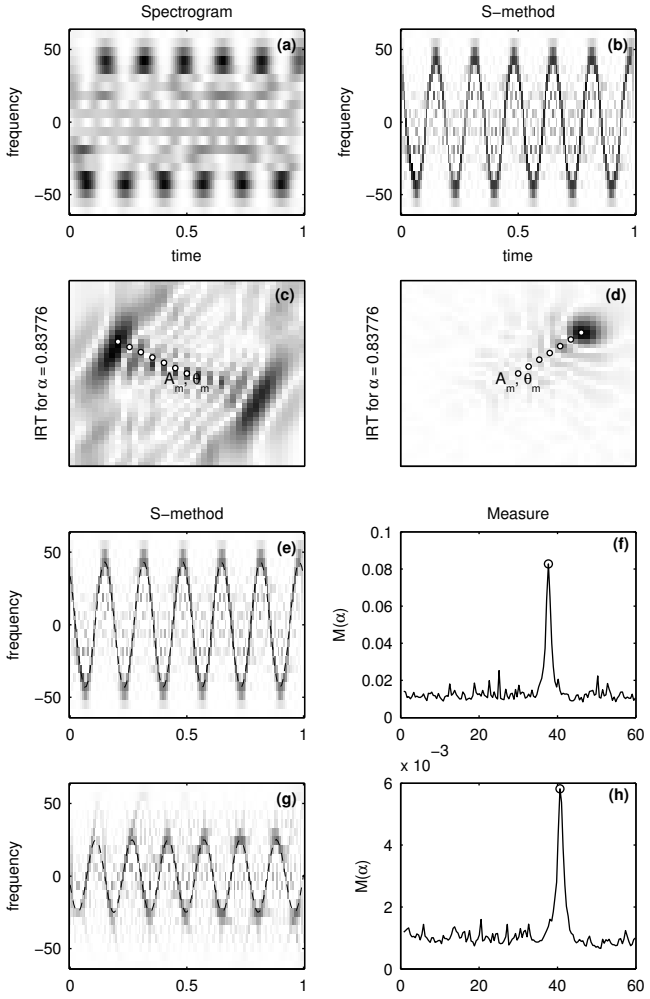

Fig. 8. Time-frequency representation of a two-component signal with fast IF changes: Spectrogram and the S-method with $L = 5$ (a), (b), respectively. The IRT for the parameter α value where the maximum of concentration measure is detected for spectrogram and the S-method (c), (d), respectively. Estimation of the first m-D component (parameter α, frequency) based on the IRT concentration measure $M(\alpha)$ (e), (f); Estimation of the second m-D component (parameter α, frequency) (g), (h).

[8] T. Sparr and B. Krane: "Micro-Doppler analysis of vibrating targets in SAR," *IEE Proc. Radar Sonar Navig*., vol 150, no. 4, pp. 277-283, Aug. 2003.

[9] B. Lyonnet, C. Ioana and M. G. Amin: "Human gait classification using micro-Doppler time-frequency signal representations," *Radar Conference, 2010 IEEE*, pp. 915 - 919, 10-14 May 2010.

[10] T. Thayaparan, S. Abrol, and E. Riseborough: "Micro-Doppler feature extraction of experimental helicopter data using wavelet and time-frequency analysis," *RADAR 2004*, *Proc. of the International Conference on Radar Systems*, 2004.

[11] T. Thayaparan, S. Abrol, E. Riseborough, L. Stanković, D. Lamothe and G. Duff: "Analysis of radar micro-Doppler signatures from experimental helicopter and human data," *IET Proceedings Radar Sonar Navig.*, vol. 1, no. 4, pp. 288-299, Aug. 2007.

[12] J. Li, and H. Ling: "Application of adaptive chirplet representation for ISAR feature extraction from targets with rotating parts," *IEE Proc. Radar, Sonar, Navig.*, vol.150, no.4, pp.284-291, August 2003.

[13] T. Thayaparan, P. Suresh and S. Qian: "Micro-Doppler Analysis of Rotating Target in SAR," *IET Signal Processing*, vol. 4, no. 3, pp 245-255, 2010.

[14] T. Thayaparan, L. Stanković and I. Djurović: "Micro-Doppler Based Target Detection and Feature Extraction in Indoor and Outdoor Environments," *J. of the Franklin Institute*, vol. 345, no. 6, pp 700-722, Sept. 2008.

[15] V. C. Chen, and H. Ling: *Time-frequency transforms for radar imaging and signal analysis*, Boston, USA: Artech House, 2002.

[16] Y. Wang, H. Ling, and V. C. Chen, "ISAR motion compensation via adaptive joint time-frequency techniques," *IEEE Trans. Aerosp. Electron. Syst.*, vol. 38, no. 2, pp. 670-677, 1998.

[17] LJ. Stanković, V. Popović-Bugarin and F. Radenović, "Genetic algorithm for rigid body reconstruction after micro-Doppler removal in the radar imaging analysis," *Signal Processing*, vol. 93, no. 7, 1921-1932, July 2013.

[18] T. Thayaparan, L. Stanković, M. Daković, V. Popović: "Micro-Doppler parameter estimation from a fraction of the period," *IET Signal Processing*, vol. 4, no. 3, pp. 201 - 212, Jan. 2010.

[19] L. Liu, D. McLernon, M. Ghogho, W. Hu, and J. Huang, "Ballistic missile detection via micro-Doppler frequency estimation from radar return," *Digital Signal Processing*, vol. 22, no. 1, pp. 87-95, Jan. 2012.

[20] V. V. Lukin, A. A. Roenko, A. V. Totsky, and I. Djurović, "Robust DFT-based signal processing in Micro-Doppler radars," *In Proc. of International Kharkov Symposium on Physics and Engineering of Microwaves, Millimeter and Submillimeter Waves (MSMW)*, 21-26 June 2010.

[21] Y. Luo, Q. Zhang, C. Qiu, X. Liang, and K. Li "Micro-Doppler effect analysis and feature extraction in ISAR imaging with stepped-frequency chirp signals," *IEEE Trans on Geoscience and Remote Sensing* , vol. 48, no. 4, pp. 2087 – 2098, April 2010

[22] X. Bai, M. Xing, F. Zhou, G. Lu, and Z. Bao, "Imaging of micromotion targets with rotating parts based on empirical-mode decomposition," *IEEE Trans on Geoscience and Remote Sensing* , vol. 46, no. 11, pp. 3514 – 3523, Nov. 2008

[23] R. M. Narayanan, "Through-wall radar imaging using UWB noise waveforms," *Journal of the Franklin Institute*, vol. 345, no. 6, pp. 659-678, Sept. 2008.

[24] J. Misiurewicz, K. Kulpa, and Z. Czekala: "Analysis of recorded helicopter echo," *IEE Radar 98, Proceedings*, pp. 449-453.

[25] S. L. Marple: "Special time-frequency analysis of helicopter Doppler radar data," in *Time-Frequency Signal Analysis and Processing*, ed. B. Boashash, Elsevier 2004.

[26] P. Suresh, T. Thayaparan, T. Obulesu, and K. Venkataramaniah: "Extracting micro-Doppler radar signatures from rotating targets using Fourier-Bessel Transform and Time-Frequency analysis," in press, *IEEE Geoscience and Remote Sensing*, 2014.

[27] S. Barbarossa, "Analysis of multicomponent LFM signals by a combined Wigner-Hough transform," *IEEE Trans. on Signal Processing*, vol. 43, no. 6, pp. 1511-1515, June 1995.

[28] S. Barbarosa and O. Lemoine, "Analysis of nonlinear FM signals by pattern recognition of their time-frequency representation," *IEEE Signal Processing Letters*, vol. 3, no. 4, pp. 112-115, Apr. 1996.

[29] L. Stanković, T. Thayaparan, M. Daković, and V. Popović-Bugarin, "Micro-Doppler removal in the radar imaging analysis," *IEEE Trans. on Aerospace and Electronics Systems*, vol. 49, no. 2, pp. 1234-1250, Apr. 2013.

[30] L. Stanković, T. Thayaparan and I. Djurović, "Separation of target rigid body and micro-Doppler effects in ISAR Imaging," *IEEE Trans. on Aerospace and Electronics Systems*, vol. 42, no. 7, pp. 1496-1506, 2006.

[31] B. Ristic and B. Boashash, "Kernel design for time-frequency signal analysis using the Radon transform," *IEEE Trans. on Signal Processing*, vol. 41, no. 5, May 1993, pp. 1996-2008.

[32] S. Stanković, I. Djurović, and I. Pitas, "Watermarking in the space /spatial-frequency domain using two-dimensional Radon-Wigner distribution," *IEEE Trans. on Image Processing*, vol. 10, no. 4, pp. 650-658, Apr. 2001.

[33] J. C. Wood and D. T. Barry, "Linear signal synthesis using the Radon-Wigner distribution," *IEEE Trans. on Signal Processing*, vol. 42, no. 8, pp. 2105-2111, Aug. 1994.

[34] J.C. Wood and D.T. Barry, "Radon transformation of time-frequency distributions for analysis of multicomponent signals," *IEEE Trans. on Signal Processing*, vol. 42, no. 11, pp.3166-3177, Nov. 1994.

[35] L. Stanković, "A measure of some time-frequency distributions concentration," *Signal Processing*, vol.81, no.3, pp. 621-631, Mar. 2001.

[36] I. Daubechies, M. Defrise, and C. De Mol, "An iterative thresholding algorithm for linear inverse problems with a sparsity constraint," *Communications on pure and applied mathematics*, vol. 57, no. 11, pp. 1413–1457, 2004.

[37] D. L. Donoho, "Compressed sensing," *IEEE Transactions on Information Theory*, vol. 52, no. 4, pp. 1289–1306, 2006.

[38] Q. Wang, M. Pepin, R. J. Beach, R. Dunkel, T. Atwood, B. Santhanam, W. Gerstle, A. W. Doerry, and M. M. Hayat, "SAR-based vibration estimation using the discrete fractional Fourier transform," *IEEE Trans. Geosci. Remote Sens.*, vol. 50, no. 10, pp. 4145-4156, Oct. 2012.

[39] I. Djurović, T. Thayaparan, and LJ. Stanković, "Adaptive Local Polynomial Fourier Transform in ISAR," *EURASIP Journal on Applied Signal Processing*, Vol. 2006, Article ID 36093.
[40] T. Alieva, M.J. Bastiaans, "Wigner distribution and fractional Fourier transform," Signal Processing and its Applications, Sixth International, Symposium on. 2001 , vol.1, no., pp.168,169 vol.1, 2001 doi: 10.1109/ISSPA.2001.949803.
[41] T. Alieva, M.J. Bastiaans, L. Stankovic, "Signal reconstruction from two close fractional Fourier power spectra," Signal Processing, IEEE Transactions on , vol.51, no.1, pp.112,123, Jan. 2003 doi: 10.1109/TSP.2002.806593
[42] L. Stanković, M. Daković, and T. Thayaparan, *Time-Frequency Signal Analysis With Applications*, Boston: Artech House, 2013.
[43] L. Stanković, S. Stanković and M. Daković, "From the STFT to the Wigner Distribution," *IEEE Signal Processing Magazine*, vol.31, no.3, May 2014, pp.163,174
[44] G.T. Herman, *Image Reconstruction from Projections: The Fundamentals of Computerized Tomography*, New York: Academic Press, 1980.
[45] L. Stanković, M. Daković, and S. Vujović, "Estimation of sinusoidally modulated signal parameters based on the inverse Radon transform," *in proc. of* 8*th International Symposium on Image and Signal Processing and Analysis (ISPA 2013),* September 4-6, 2013, Trieste, Italy.

Ljubiša Stanković (*M'91–SM'96–F'12*) was born in Montenegro in 1960. He received the B.S. degree in EE from the University of Montenegro (UoM), the M.S. degree in Communications from the University of Belgrade and the Ph.D. in Theory of Electromagnetic Waves from the UoM. As a Fulbright grantee, he spent 1984-1985 academic year at the Worcester Polytechnic Institute, USA. Since 1982, he has been on the faculty at the UoM, where he has been a full professor since 1995. In 1997-1999, he was on leave at the Ruhr University Bochum, Germany, supported by the AvH Foundation. At the beginning of 2001, he was at the Technische Universiteit Eindhoven, The Netherlands, as a visiting professor. He was vice-president of Montenegro 1989-90. During the period of 2003-2008, he was Rector of the UoM. He is Ambassador of Montenegro to the UK, Ireland and Iceland. His current interests are in Signal Processing. He published about 400 technical papers, more than 135 of them in the leading journals, mainly the IEEE editions. Prof. Stanković received the highest state award of Montenegro in 1997, for scientific achievements. He was a member the IEEE SPS Technical Committee on Theory and Methods, an Associate Editor of the *IEEE Transactions on Image Processing*, the *IEEE Signal Processing Letters* and numerous special issues of journals. Prof. Stanković was an Associate Editor of the *IEEE Transactions on Signal Processing*. He is a member of the National Academy of Science and Arts of Montenegro (CANU) since 1996 and a member of the European Academy of Sciences and Arts.

Miloš Daković was born in 1970, Nikšić, Montenegro. He received the B.S. degree in 1996, the M.Sc. degree in 2001 and the Ph.D. degree in 2005, all at the University of Montenegro in EE. He is an associate professor at the University of Montenegro. His research interests are signal processing, time-frequency signal analysis and radar signal processing. He is a member of the Time-Frequency Signal Analysis Group (www.tfsa.ac.me) at the University of Montenegro where he was involved in several research projects supported by Volkswagen foundation, Montenegrian Ministry of Science and Canadian Government (DRDC).

Thayananthan Thayaparan earned a B.Sc. (Hons.) in physics at the University of Jaffna, Srilanka, an M.Sc. in physics at the University of Oslo, Norway in 1991, and a Ph.D. in atmospheric physics at the University of Western Ontario, Canada in 1996. From 1996 to 1997, he was employed as a Postdoctoral Fellow at the University of Western Ontario. In 1997, he joined the Defence Research and Development Canada - Ottawa, Department of National Defence, Canada, as a Defence Scientist. His research interests include advanced radar signal and image processing methodologies and techniques against SAR/ISAR and HFSWR problems such as detection, classification, recognition, and identification. His current research includes synthetic aperture radar imaging algorithms, time-frequency analysis for radar imaging and signal analysis, radar micro-Doppler analysis, and noise radar technology. Dr. Thayaparan is a Fellow of the IET (Institute of Engineering & Technology). Currently, he is an Adjunct Professor at McMaster University. Dr. Thayaparan received IET Premium Award for Signal Processing for the best paper published in 2009-2010. Dr. Thayaparan is currently serving in the Editorial Board of *IET Signal Processing*. He has authored or coauthored over 174 publications in journals, proceedings, and internal distribution reports. As a principal writer, he wrote 3 editorials for the international journals *IET Signal Processing* (Institute of Engineering and Technology) and *IET Radar, Sonar & Navigation*.

Vesna Popović-Bugarin was born in 1978, in Podgorica, Montenegro. She received the B.S. degree in 2001, the M.S. degree in 2005, and the Ph.D. degree in 2009, all at the University of Montenegro, in EE. She is currently assistant professor at the Faculty of Electrical Engineering, University of Montenegro. Her research interests include time-frequency signal analysis, SAR/ISAR imaging, micro-Doppler analysis and parameter estimation. She has published 20 scientific papers (8 in international journals, 10 in international conferences and 2 in domestic conference). More information about Vesna Popović-Bugarin can be found on http://www.tfsa.ac.me/vesna.html.